Electronic Supplementary Information for

Size tunable bimetallic nickel-zinc nitride as multi-functional co-catalyst on nitrogen doped titania boost solar energy conversions

Weiliang Qi,[ab] Xiangjian Meng,[ab] Samira Adimi,[ab] Haichuan Guo,[ab] Tiju Thomas,[c] Fei Li,[d] Heng Jiang,[d] Siqi Liu*[ab] and Minghui Yang*[ab]

[a] Ningbo Institute of Materials Technology & Engineering, Chinese Academy of Sciences, Ningbo 315201, P.R. China.

[b] Center of Materials Science and Optoelectronics Engineering, University of Chinese Academy of Sciences, Beijing 100049, P.R. China.

[c] Department of Metallurgical and Materials Engineering, Indian Institute of Technology Madras, Adyar, Chennai 600036, Tamil Nadu, India.

[d] College of Chemistry, Chemical Engineering and Environment Engineering, Liaoning Shihua University, Fushun 113001, China.

*[ab] Correspondence Author: Dr. Siqi Liu; Prof. Minghui Yang;

E-mail addresses: liusiqi@nimte.ac.cn; myang@nimte.ac.cn;

Table of contents

I. Experimental Procedures

Preparation of TiO_2 precursor, TiO_2 and N-TiO_2 nanospheres: 1.98 g 1-Hexadecylamine (HAD) was dissolved in 200 mL absolute ethanol with 1.6 mL deionized water and mixture were stirred for 30 min. Further 4.5 mL Titanium tetraisopropanolate (TIP) as titanium source was dripped into the mixture quickly, while the mix was being stirred. The white precursor suspension was kept static for 18 h. The white product was collected by centrifugal separation and washed by deionized water and anhydrous ethanol several times. After harvesting, the sample was dried at 60 ^oC for 12h in an oven. The precursor was put into the crucible and calcined in a muffle furnace at 550 °C for 2 h using a heating rate of 5 °C/min and cooled naturally to room temperature. The white sample is as-prepared pure TiO_2. Subsequently, the TiO_2 sample was transferred in a quartz boat and nitrided in NH_3 flow (99.999%) of 100 sccm at 550 ^oC with heating rate 5 $^oC\ min^{-1}$ maintained for 2h. The sample was cooled down to the room temperature in the same NH_3 flow. The grey sample is the N-TiO_2 (Nitrogen doping TiO_2) nanospheres.

Electrochemical Measurements: The electrochemical tests were conducted on an electrochemical workstation (CHI760E, CH Instrument) with a conventional three electrode cell. A Pt plate was employed as the counter electrode and an Ag/AgCl electrode was used as the reference electrode. The working electrode was prepared on fluorine-doped tin oxide (FTO) glass. The boundary of FTO glass was protected using the scotch tape. The 5 mg sample were dispersed into 300 µL N, N-dimethyl benzamide solution with 0.1% nafion solution. After ultrasonication for 30 min (i.e. to form a paste-like suspension), the slurry was obtained. Then, 30 µL of slurry was spread onto the pretreated FTO glass. The working electrode was further dried at 60 ^oC for 20 min to improve adhesion. Then, the scotch tape was unstuck, and the uncoated part of the electrode was isolated with epoxy resin. The exposed area of the working electrode was 0.25 cm^2. The photocurrent measurements were carried out with the electrolyte was 0.2 M aqueous Na_2SO_4 solution. The electrochemical impedance spectroscopy (EIS) measurements were performed in 0.2 M aqueous Na_2SO_4 solution by applying an AC voltage with -1.3 mV amplitude in a frequency range from 0.01 Hz to 100K Hz. The polarization curve is performed as mentioned above using three-electrode system, while the bias sweep range is from -1.5 to -0.2 V vs Ag/AgCl the electrolyte was 0.2 M aqueous Na_2SO_4 solution. Mott-Schottky experiments were obtained on AutoLab workstation with the potential ranged from -0.8 V to 0.2 V (vs. Ag/AgCl) under three different frequencies of 500 Hz, 700 Hz, and 900 Hz and the electrolyte was 0.2 M aqueous Na_2SO_4 solution (pH = 6.8) without additive. Cyclic voltammograms were measured in 0.5 M KCl aqueous solution containing 10.0 mM $K_3[Fe(CN)_6]/K_4[Fe(CN)_6]$ with the scanning rate of 100 mV/s in the same three-electro system. Specific capacitance performances (Cyclic voltammetry) of the samples were carried out using the rotating ring-disk electrode (RRDE) as the working electrode. 30 µL of the same slurry was pipetted onto a clean RRDE surface and dried at 40 ^oC for 30 min (about 2.5 mg/cm^2). The specific capacitance is calculated according the formula of $C = \frac{\int IdV}{V\Delta E}$, Where *C (F)* is the total capacitance, $\int IdV$ is the areas of close curves, ΔE is the electrochemical window, *v* is the scanning rate.

Computational details: The Density Functional Theory (DFT) is performed for structural relaxation and investigating the electronic properties in a basis set of plane waves, adopting GGA-PBE exchange-correlation functionals [1, 2], implemented in Quantum Espresso Package [3]. The electron-core interactions are taken into account considering Projector Augmented Wave (PAW) pseudo-potentials [4]. We have used the crystal structure determined by our group in room temperature and using of X-ray diffraction pattern for starting calculation. The full relaxation of unit cells and atomic coordinates are allowed until the total energy scf accuracy of 10^{-6} eV $atom^{-1}$ and the residual force below 0.001 eV/Å., with 40 Ry cutoff energy and a 6×6×6 k-point mesh, generated by the MontkhorstePack method [1]. The BFGS quasi-newton algorithm [5] is used for calculating the geometry of the ground state.

Turnover frequency (TON): The turnover number is calculated by using the following equations [6]:

$$\mathrm{TON} = \frac{\text{Moles of evolved } H_2}{\text{Moles of } Ni_3ZnN \text{ on photocatalyst}}$$

Photocatalytic reduction of Cr(VI): 30 mg of catalyst and 40 mg $HCOONH_4$ were added into 40 mL of the Cr(VI) solution (10 $mg{\cdot}L^{-1}$, were prepared by dissolving $K_2Cr_2O_7$ in deionized water) in a quartz vial. The suspension was stirred in dark for 1 h to establish of adsorption-desorption equilibrium between the sample and reactant. The same Xe arc lamp was used as the light source (λ > 400 nm). 2 mL of suspension was collected at a certain time interval during the process of the reaction and centrifuged to remove the catalyst completely at 10000 rpm. Afterward, the solution was analyzed on a Varian ultraviolet-visible light (UV–Vis) spectrophotometer (Hitachi U-3900). The whole experimental process was conducted under N_2 bubbling at the flow rate of 50 sccm.

II. Supplementary illustrations and explanations

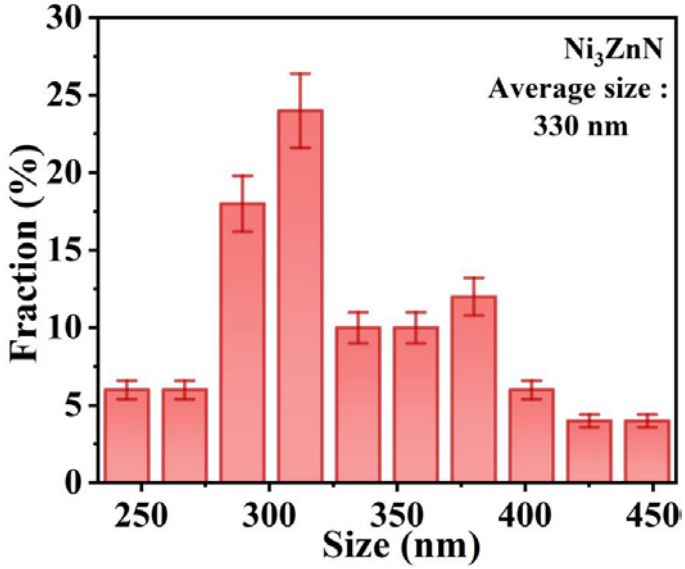

Fig. S1 The diameters statistic histogram of pure Ni_3ZnN sample.

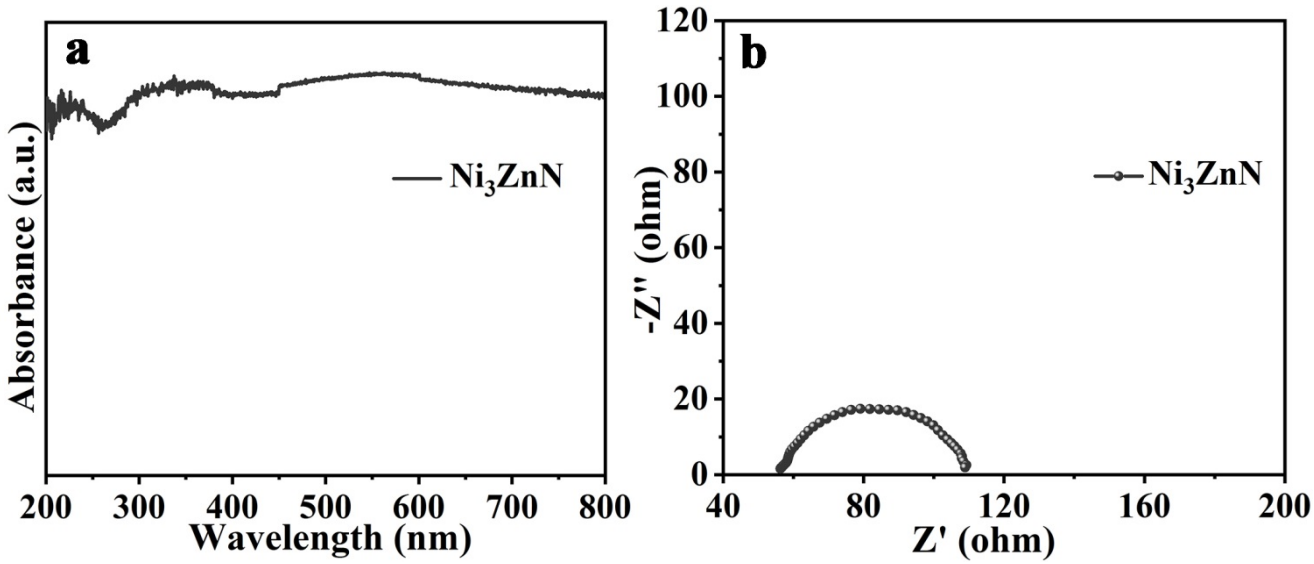

Fig. S2 (a) UV-vis absorption spectra and (b) Electrical impedance spectra of pure Ni_3ZnN sample.

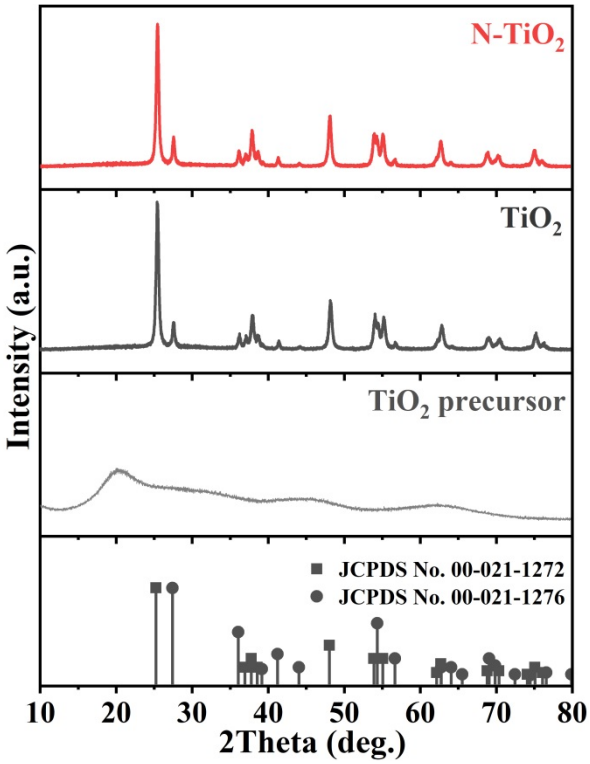

Fig. S3 XRD pattern of TiO_2 precursor, TiO_2 and N-TiO_2 samples.

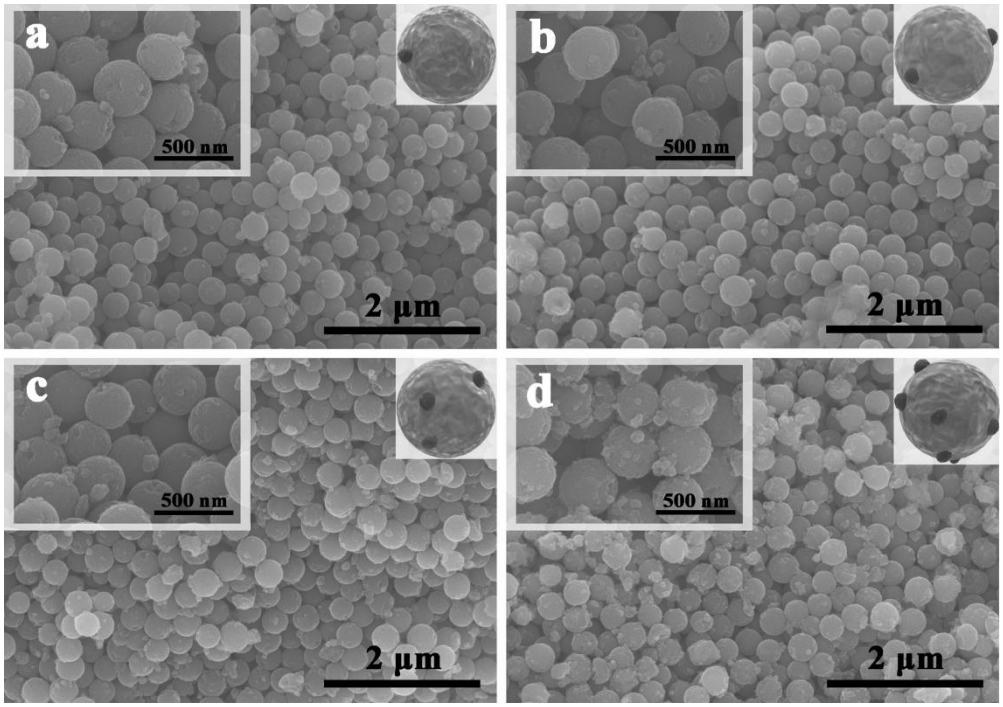

Fig. S4 SEM images of (a) N-TiO_2-1%Ni_3ZnN, (b) N-TiO_2-3%Ni_3ZnN, (c) N-TiO_2-5%Ni_3ZnN and (d) N-TiO_2-10%Ni_3ZnN.

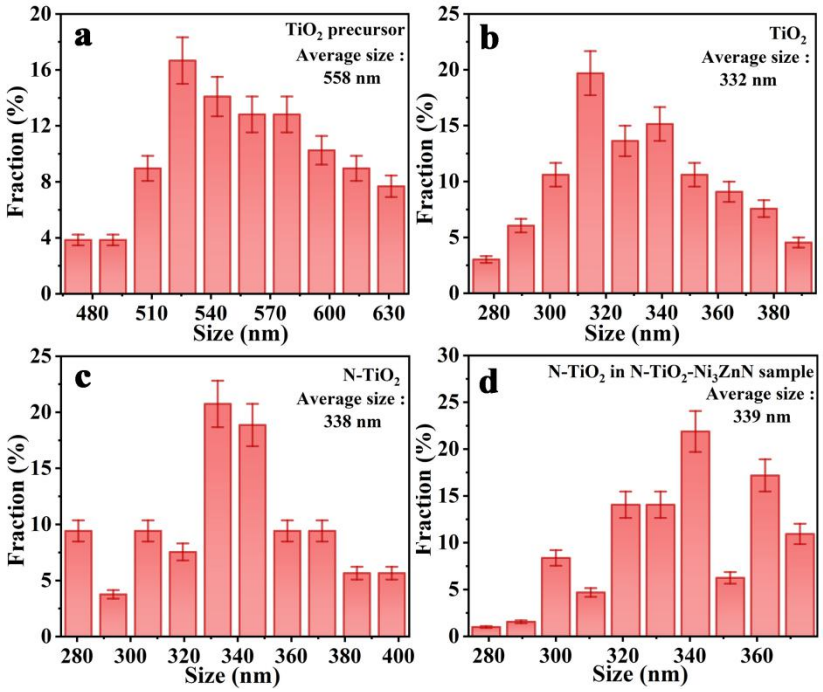

Fig. S5 The diameters statistic histogram of (a) TiO_2 precursor, (b) TiO_2, (c) N-TiO_2 and(d) N-TiO_2 in the N-TiO_2-Ni_3ZnN sample.

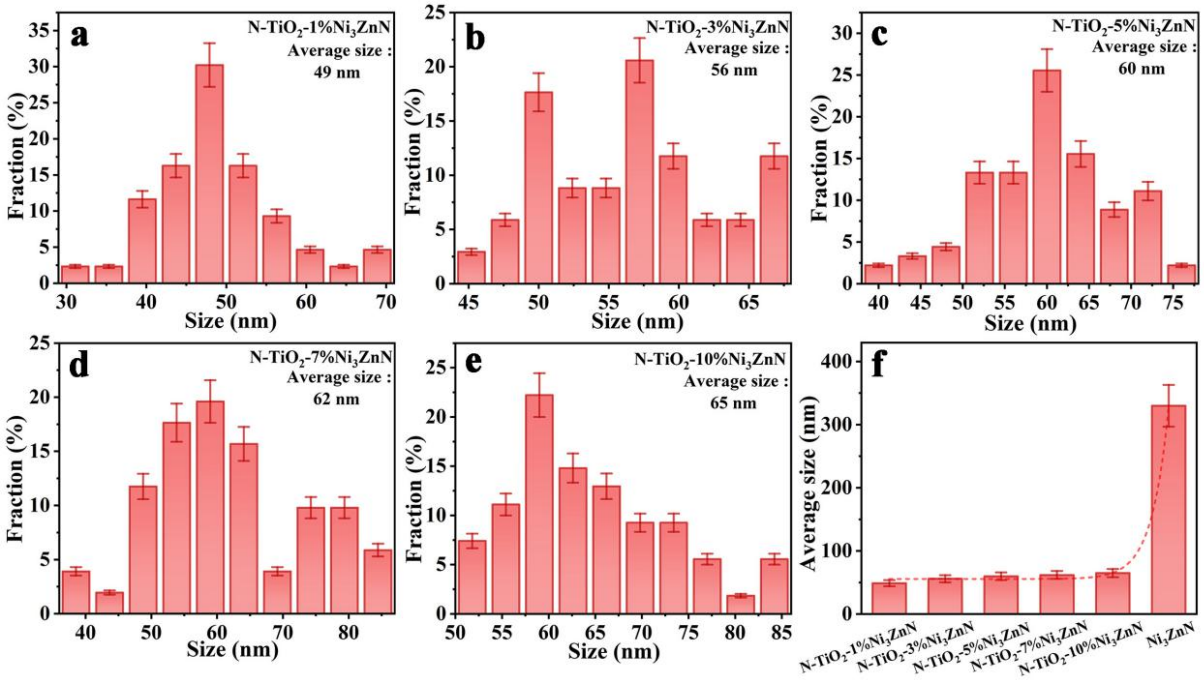

Fig. S6 The diameters statistic histogram of Ni_3ZnN in (a) N-TiO_2-1%Ni_3ZnN sample, (b) N-TiO_2-3%Ni_3ZnN sample, (c) N-TiO_2-5%Ni_3ZnN sample, (d) N-TiO_2-7%Ni_3ZnN sample and (e) N-TiO_2-10%Ni_3ZnN sample. (f) The tendency chart of Ni_3ZnN diameters.

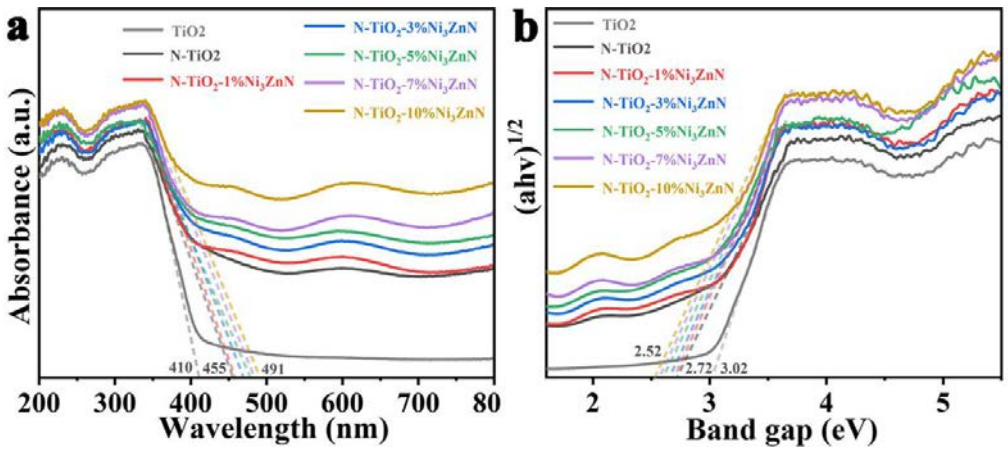

Fig. S7 (a) UV-vis absorption spectra and (b) the Tauc plots spectra of TiO_2 based samples.

Note: The bandgap (Eg) of the TiO_2 based samples can be calculated from the following equation:

$a=A(hv–Eg)^{n/2}/hv$

where a, A, Eg, h and v are the absorption coefficient, proportionality constant, band energy, Planck's constant and frequency of the incident light, respectively. n is 1 for direct gap semiconductor and n is 4 for indirect gap semiconductor [7]. In general, TiO_2 is an indirect bandgap semiconductor. Therefore, the bandgap energy of TiO_2 based samples are calculated by the intercept of the tangents on the horizontal axis in the corresponding Tauc plots of the $(ahv)^{1/2}$ *versus* photon energy (hv) in **Fig. S7** [8].

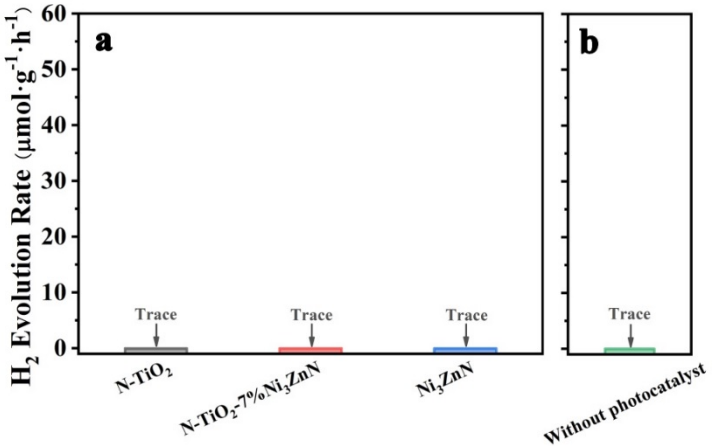

Fig. S8 The control experiments for photocatalytic H_2 evolution (a) without the irradiation and (b) without photocatalyst.

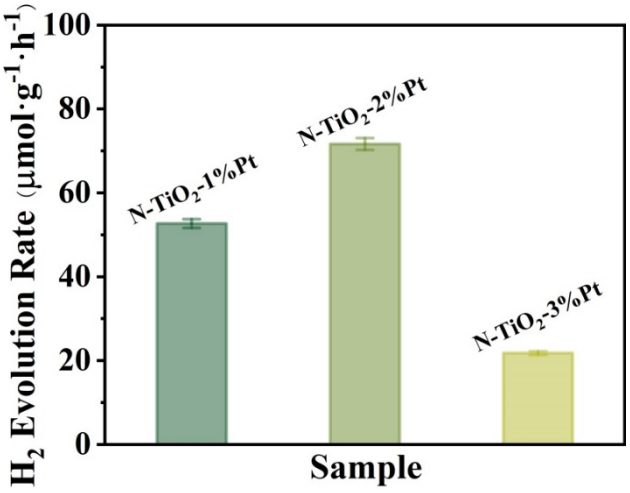

Fig. S9 The average rates of H_2 evolution under visible-light (λ≥400 nm) over a series of N-TiO_2-Pt composites.

Note: A series of N-TiO_2-Pt samples (1 wt%, 2 wt% and 3 wt%) have been synthesized *via* a photo-deposition method in a Pyrex vessel. In all cases, 20 mg N-TiO_2 and chloroplatinic acid solution (50 mM) with different volumes (20 μL, 40 μL, 60 μL) are added together in the above mentioned reaction system and illuminated for 1 h under a 300 W Xe arc lamp. And then the N-TiO_2-Pt composites are obtained. The H_2 evolution activities of a series of N-TiO_2-Pt composites are measured under the same condition with N-TiO_2-Ni_3ZnN. The optimum loading content of Pt is found to be about 2 wt % and the H_2 generation rate is 71.7 μmol g^{-1} h^{-1}.

Table S1. Representative summary on photocatalytic activity of non-noble based photocatalysts toward water splitting H_2 evolution.

Photocatalyst	**Co-catalysts/mass ratio**	**Light source**	**Reaction conditions**	**PHER rate[a]**	**Ref.**
g-C_3N_4	Ni_xP_y /5 wt%	Xe light 300W, λ>420 nm	Aqueous TEOA solution (25%)	34	[9]
g-C_3N_4	$Ni_xCo_{1-x}S_2$ / 5 wt%	White LED, λ>420 nm	Aqueous TEOA solution (15%), Eosin Y-sensitized catalyst (10mg)	9	[10]
g-C_3N_4	CoO	Xe light 300W, λ>400 nm	Aqueous lactic acid solution (10%)	3	[11]
CdS	Ni_3C /1 wt%	Xe light 350W, λ>420 nm	Aqueous solution of Na_2S (0.25 M) and Na_2SO_3 (0.25 M)	8	[12]
CdS	MoS_2 / 2 wt%	Xe light 300W, λ>420 nm	Aqueous lactic acid solution (10%)	65	[13]
CdS	Mo_2C@C / 2 wt%	Xe light 300W, λ>420 nm	Aqueous lactic acid solution (10%)	26	[14]
CdS/g-C_3N_4	$Ni(OH)_2$ / 4.76 wt%	Xe light 300W, λ>420 nm	Aqueous solution of Na_2S (0.5 M) and Na_2SO_3 (0.7 M)	26	[15]
$ZnIn_2S_4$	MoC-QDs/C / 2.5 wt%	Xe light 300W, λ>400 nm	Aqueous lactic acid solution (10%)	48	[16]
TiO_2	Mo_2C	Xe light 300W, full spectrum	Aqueous TEOA solution (10%)	25	[17]
TiO_2	TiN	Xe light 300W, full spectrum	Aqueous CH_3OH solution (30%)	12	[18]
N-TiO_2	Ni_3ZnN / 7 wt%	Xe light 300W, λ>400 nm	Aqueous TEOA solution (10%)	**33**	**This work**

Note: [a]**PHER rate** denotes the hydrogen evolution rate of times higher than pristine photocatalyst.

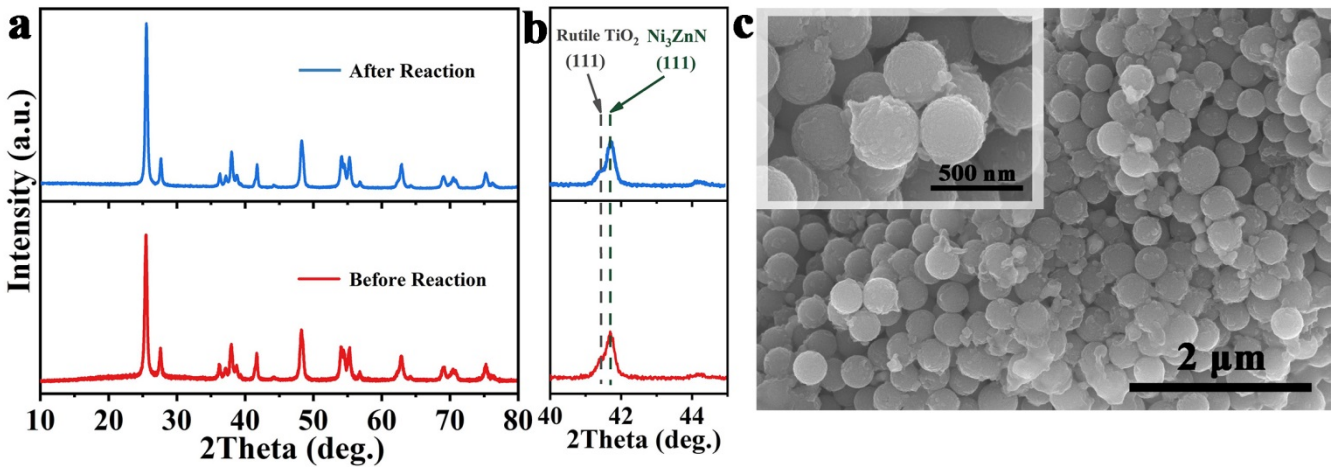

Fig. S10 (a) The XRD pattern, (b) high-resolution XRD pattern and (c) the SEM image of the used (after 24h stability examination) N-TiO_2-7%Ni_3ZnN sample.

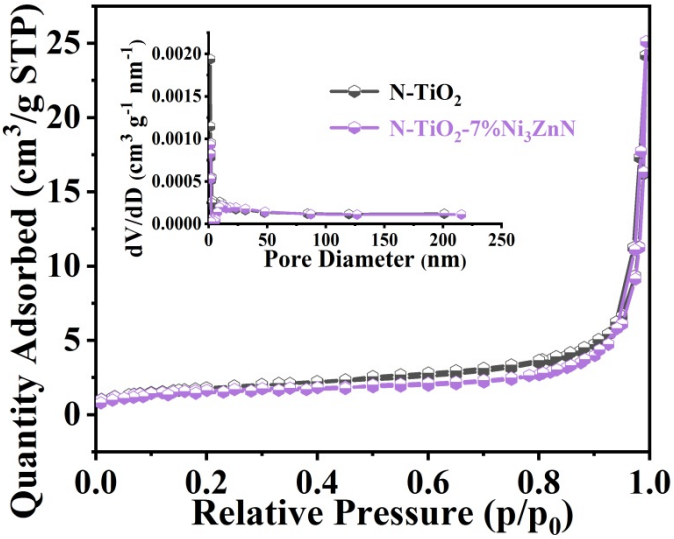

Fig. S11 N_2 adsorption–desorption isotherms and the corresponding pore size distribution curves (inset) of N-TiO_2 and N-TiO_2-7%Ni_3ZnN samples.

Table S2 Pore Structure Parameters of N-TiO_2 and N-TiO_2-7%Ni_3ZnN.

Photocatalyst	BET surface area ($m^2\ g^{-1}$)	mean pore diameter (nm)	pore volume ($cm^3\ g^{-1}$)
N-TiO_2	6.45	28.19	0.037
N-TiO_2-7%Ni_3ZnN	5.78	40.07	0.038

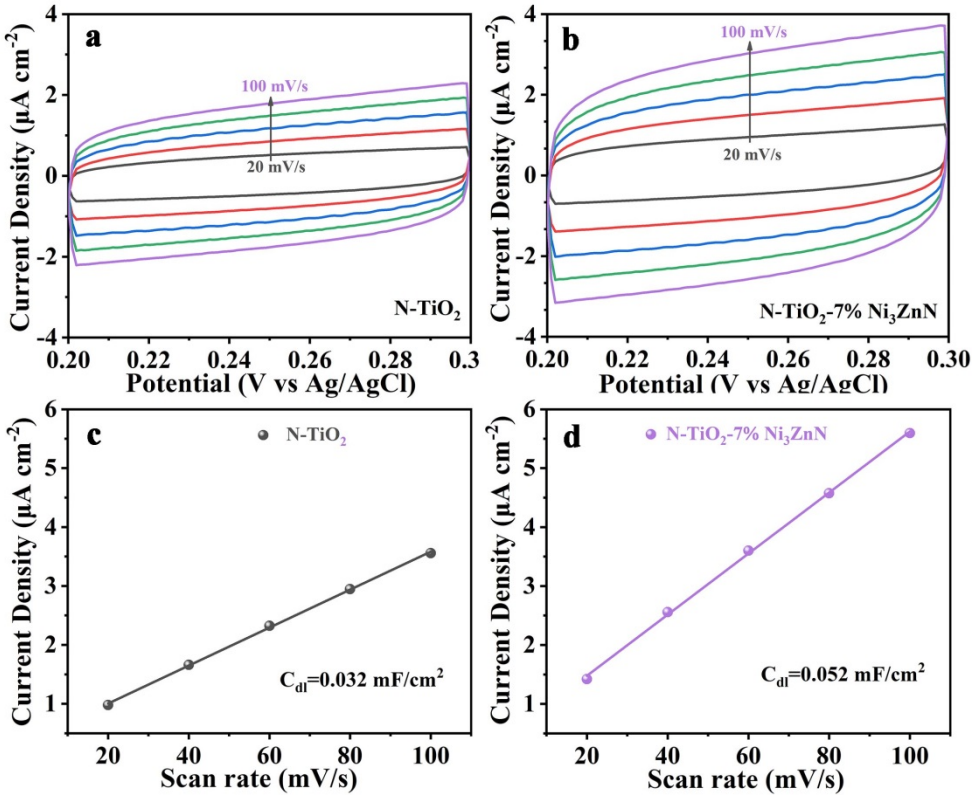

Fig. S12 Cyclic voltammetry curve with different scan rates for (a) N-TiO_2 and (b) N-TiO_2-7%Ni_3ZnN samples. Charging current density with different scan rates corresponding to (c) N-TiO_2 and (d) N-TiO_2-7%Ni_3ZnN samples.

Note: **Fig. S12** shows the CV curves of pure N-TiO_2 and N-TiO_2-7%Ni_3ZnN sample at different scan rates (from 20 mV/s to 100 mV/s) and the summary plot of areal specific capacitance under different scan rates. Meanwhile, the electrochemically active surface area (EASA) was studied by measuring the electrochemical double-layer capacitance (C_{dl}). The nanocomposite show a higher electrochemical double-layer capacitance (C_{dl}=0.052 mF cm^{-2}) than that of pure N-TiO_2 sample (C_{dl}=0.032 mF cm^{-2}). Thus, N-TiO_2-7%Ni_3ZnN sample has larger electrochemical surface area than the pure N-TiO_2 sample.

III. Supplementary References

[1] J.P. Perdew, K. Burke, M. Ernzerhof, Phys. Rev. Lett., 77 (1996) 3865-3868.

[2] J.P. Perdew, K. Burke, M. Ernzerhof, Phys. Rev. Lett., 78 (1997) 1396-1396.

[3] P. Giannozzi, S. Baroni, N. Bonini, M. Calandra, R. Car, C. Cavazzoni, D. Ceresoli, G.L. Chiarotti, M. Cococcioni, I. Dabo, A. Dal Corso, S. de Gironcoli, S. Fabris, G. Fratesi, R. Gebauer, U. Gerstmann, C. Gougoussis, A. Kokalj, M. Lazzeri, L. Martin-Samos, N. Marzari, F. Mauri, R. Mazzarello, S. Paolini, A. Pasquarello, L. Paulatto, C. Sbraccia, S. Scandolo, G. Sclauzero, A.P. Seitsonen, A. Smogunov, P. Umari, R.M. Wentzcovitch, J. Phys.: Condens. Matter, 21 (2009) 395502.

[4] P.E. Blöchl, Phys. Rev. B, 50 (1994) 17953-17979.

[5] B.J.F. Bonnans, J.C. Gilbert, C. Lemaréchal, C.A. Sagastizábal, IEEE T. Automat. Contr., 51 (2006) 541-541.

[6] Z. Sun, H. Zheng, J. Li, P. Du, Energ. Environ. Sci., 8 (2015) 2668-2676.

[7] K. Chen, X.-M. Zhang, X.-F. Yang, M.-G. Jiao, Z. Zhou, M.-H. Zhang, D.-H. Wang, X.-H. Bu, Appl. Catal. B-Environ., 238 (2018) 263-273.

[8] H. Huang, Y. Song, N. Li, D. Chen, Q. Xu, H. Li, J. He, J. Lu, Appl. Catal. B-Environ., 251 (2019) 154-161.

[9] Z. Sun, M. Zhu, M. Fujitsuka, A. Wang, C. Shi, T. Majima, ACS Appl. Mater. Interfaces, 9 (2017) 30583-30590.

[10] K. Fan, Z. Jin, H. Yang, D. Liu, H. Hu, Y. Bi, Sci Rep, 7 (2017) 7710.

[11] Z. Mao, J. Chen, Y. Yang, D. Wang, L. Bie, B.D. Fahlman, ACS Appl. Mater. Interfaces, 9 (2017) 12427-12435.

[12] S. Ma, Y. Deng, J. Xie, K. He, W. Liu, X. Chen, X. Li, Appl. Catal. B-Environ., 227 (2018) 218-228.

[13] B. Han, S. Liu, N. Zhang, Y.-J. Xu, Z.-R. Tang, Appl. Catal. B-Environ., 202 (2017) 298-304.

[14] Y.-X. Pan, J.-B. Peng, S. Xin, Y. You, Y.-L. Men, F. Zhang, M.-Y. Duan, Y. Cui, Z.-Q. Sun, J. Song, ACS Sustain. Chem. Eng., 5 (2017) 5449-5456.

[15] Z. Yan, Z. Sun, X. Liu, H. Jia, P. Du, Nanoscale, 8 (2016) 4748-4756.

[16] F. Gao, Y. Zhao, L. Zhang, B. Wang, Y. Wang, X. Huang, K. Wang, W. Feng, P. Liu, J. Mater. Chem. A, 6 (2018) 18979-18986.

[17] X. Yue, S. Yi, R. Wang, Z. Zhang, S. Qiu, J. Mater. Chem. A, 5 (2017) 10591-10598.

[18] X. Yu, Z. Zhao, D. Sun, N. Ren, L. Ding, R. Yang, Y. Ji, L. Li, H. Liu, Chem. Commun., 54 (2018) 6056-6059.